Deletion of IFT20 in the mouse kidney causes misorientation of the mitotic spindle and cystic kidney disease

Julie A. Jonassen,[2] Jovenal San Agustin,[1] John A. Follit,[1] and Gregory J. Pazour[1]

[1]Program in Molecular Medicine, University of Massachusetts Medical School, Worcester, MA 01605
[2]Department of Physiology, University of Massachusetts Medical School, Worcester, MA 01655

Primary cilia project from the surface of most vertebrate cells and are thought to be sensory organelles. Defects in primary cilia lead to cystic kidney disease, although the ciliary mechanisms that promote and maintain normal renal function remain incompletely understood. In this work, we generated a floxed allele of the ciliary assembly gene *Ift20*. Deleting this gene specifically in kidney collecting duct cells prevents cilia formation and promotes rapid postnatal cystic expansion of the kidney. Dividing collecting duct cells in early stages of cyst formation fail to properly orient their mitotic spindles along the tubule, whereas nondividing cells improperly position their centrosomes. At later stages, cells lacking cilia have increased canonical Wnt signaling and increased rates of proliferation. Thus, IFT20 functions to couple extracellular events to cell proliferation and differentiation.

Introduction

Nearly all cells in vertebrate organisms have nonmotile primary cilia projecting from the surface. In mice, severe defects in ciliary assembly cause embryonic lethality at mid-gestation, whereas milder defects lead to a syndrome of phenotypes including cystic kidney disease, liver cysts and fibrosis, polydactyly, and defects of the pancreas, brain, and eye. The primary cilium is considered to be a sensory organelle that relays information about the extracellular environment to the intracellular milieu, controlling aspects of cell physiology such as proliferation and differentiation (Satir and Christensen, 2007).

Primary cilia are evident on the epithelial cells lining kidney ducts and tubules. Ciliary defects underlie nearly all types of cystic kidney disease in humans including autosomal dominant and autosomal recessive polycystic kidney disease (PKD; Pazour, 2004). In PKD, increases in kidney tubular diameter cause enlargement of the kidneys and loss of surrounding nephrons. It is thought that increased proliferation of mutant epithelial cells (Igarashi and Somlo, 2002) along with defects in planar cell polarity play roles in the development of PKD (Simons et al., 2005; Fischer et al., 2006). The function of the primary cilium in controlling the architecture of the kidney and preventing cyst formation is not understood.

Most eukaryotic cilia and flagella are assembled and maintained by intraflagellar transport (IFT). During IFT, large protein complexes called IFT particles are transported along the ciliary microtubules under the ciliary membrane and carry precursors from the site of synthesis in the cell body to the site of ciliary assembly. The particles themselves comprise ~20 unique subunits organized into A and B complexes (Rosenbaum and Witman, 2002; Scholey, 2003). Here, we characterize the function of IFT20, a complex B subunit, by creating a floxed allele of *Ift20* and deleting this gene specifically in kidney collecting duct epithelium. We show that IFT20 plays roles in controlling Wnt signaling and cell proliferation and is required for proper positioning of the centrosome in nondividing cells and correct orientation of the mitotic spindle in dividing cells.

J.A. Jonassen, J. San Agustin, and J.A. Follit contributed equally to this paper.

Correspondence to Gregory J. Pazour: gregory.pazour@umassmed.edu

Abbreviations used in this paper: DBA, *Dolichos biflorus* agglutinin; e, embryonic day; GAPDH, glyceraldehyde 3-phosphate dehydrogenase; HNF, hepatocyte nuclear factor; IFT, intraflagellar transport; p, postnatal day; PKD, polycystic kidney disease; qPCR, quantitative real-time PCR; Tcf, T cell factor.

The online version of this article contains supplemental material.

The Rockefeller University Press $30.00
J. Cell Biol. Vol. 183 No. 3 377–384
www.jcb.org/cgi/doi/10.1083/jcb.200808137

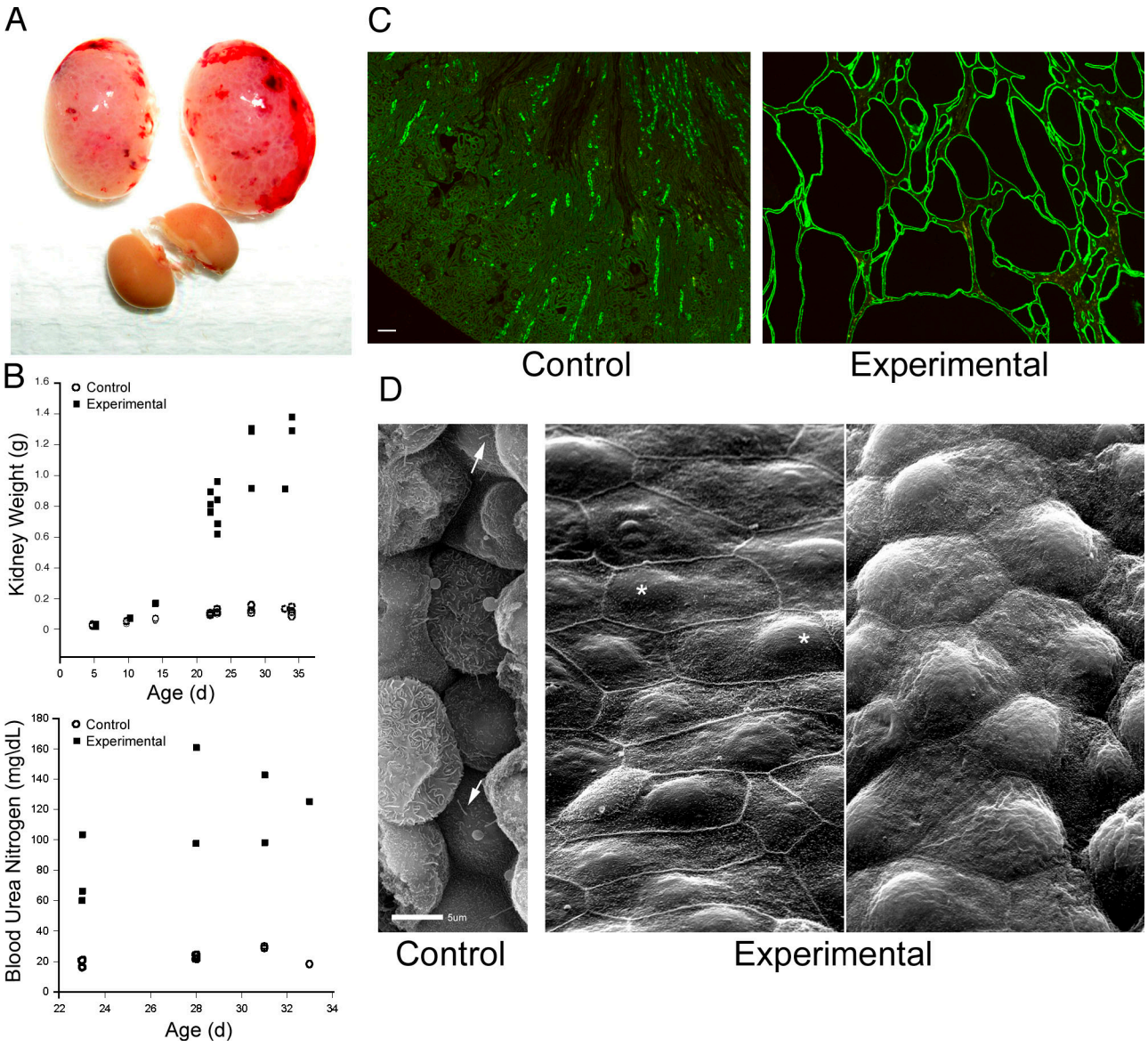

Figure 1. **Deletion of *Ift20* in mouse kidney.** (A) Gross morphology of experimental kidneys (top pair) and control kidneys at p23. (B) Mean weight of kidneys and blood urea nitrogen levels of control and experimental animals. Each symbol represents one animal. The symbols at 5 and 10 d were slightly offset. (C) Adult (p23) kidneys stained with DBA (green). (D) Scanning EM images of control and experimental kidneys. Arrows indicate cilia and asterisks indicate nuclei. Bars: (C) 100 µm; (D) 5 µm.

Results and discussion

Deletion of IFT20 in kidney leads to cystic kidney disease

Ift20 is required for embryonic viability (not depicted); thus, to characterize the function of IFT20 in the kidney, we created a floxed allele (Fig. S1, available at http://www.jcb.org/cgi/content/full/jcb.200808137/DC1) and used HoxB7-Cre to delete IFT20 in collecting ducts. HoxB7-Cre is first expressed in the mesonephric duct on embryonic day (e) 9.5 and is strongly expressed in all ureteric bud epithelial cells by e12.5 (Yu et al., 2002). The ureteric bud gives rise to the kidney collecting duct epithelium, the Wolffian duct, and the ureteral epithelium. Thus HoxB7-Cre should delete IFT20 in the collecting ducts but not in the other segments of the uriniferous tubule.

Embryonic renal deletion of *Ift20* leads to postnatal bilateral kidney enlargement (Fig. 1, A and B). At postnatal day (p) 5, control and experimental kidneys are similar in size. By p10, *Ift20* mutant kidneys are slightly enlarged, then rapidly expand to ~10 times their normal weight by p23. The enlargement is caused by cystic expansion of the collecting ducts (Fig. 1 C), such that by p23, most of the kidney is replaced by collecting duct epithelium, fluid filled cysts (Fig. 1 C), and fibrotic material (Fig. S2, available at http://www.jcb.org/cgi/content/full/jcb.200808137/DC1). Blood urea nitrogen levels are more than three times higher than normal in mutant mice, which is consistent with renal failure (Fig. 1 B). Cyst-lining cells lack primary cilia and vary in appearance between cysts (Fig. 1 D). Some cysts contain flat cells with prominent microvilli at cell borders (Fig. 1 D, middle), whereas other cysts have domed cells with

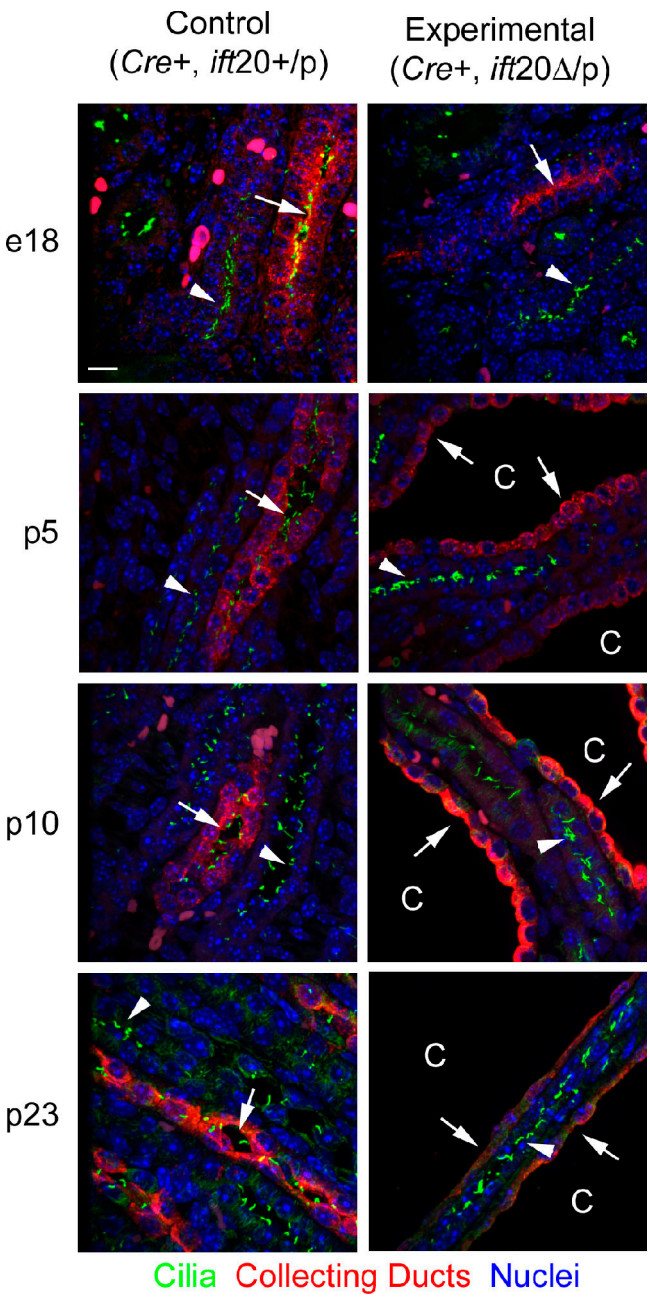

Figure 2. **Relationship between cilia loss and cystic expansion.** Kidneys from control and experimental animals were stained for cilia (611β1, green), collecting ducts (aquaporin-2, red), and nuclei (DAPI, blue) at e18, which is the day before birth, and p5, p10, and p23. Arrows indicate collecting ducts and arrowheads indicate ciliated nephrons near collecting ducts; cysts and dilated ducts are indicated by a "C." Images are maximum projections of 16 confocal z images taken 0.5 µm apart. Bar, 10 µm.

less pronounced microvilli (Fig. 1 D, right). These differences may reflect the collecting duct region from which the cysts originate, as collecting duct cells at the proximal end are flat, whereas the more distal cells are domed. Nuclei were often asymmetrically positioned (Fig. 1 D, middle, asterisk).

To examine the temporal sequence of events leading to cystic disease in this model, we examined control and mutant kidneys at e18 (the day before birth) and at p5, p10, and p23 (Fig. 2). HoxB7-Cre is highly expressed in collecting duct precursor cells by e12.5 (Yu et al., 2002). Therefore, *Ift20* should be deleted by e18, and indeed, cilia were almost completely absent from e18 experimental collecting duct epithelia, whereas control collecting ducts were highly ciliated (Fig. 2). Although cilia were absent in e18 mutant collecting ducts, no tubular dilation was observed. 5 d later, some collecting duct dilation was observed in experimental mice (Fig. 2, p5), and clear cysts could be found at p10 and beyond (Fig. 2, p10 and p23). Cyst formation initiated in the medulla near the base of the papilla and spread outwardly. At all time points, noncollecting duct epithelia were highly ciliated in both control and experimental mice, which supports the specificity of HoxB7-Cre to delete IFT20 only in collecting ducts. Moreover, all cysts were positive for collecting duct markers (aquaporin-2 or *Dolichos biflorus* agglutinin [DBA]) and lacked cilia, which indicates that they arose only from cells where IFT20 was deleted.

Deletion of IFT20 affects cellular architecture and Wnt signaling

Mitotic spindles in normal kidney tubules have a stereotypical orientation, with the axis of the spindle parallel to the long axis of the tubule and the metaphase chromosomes aligned perpendicular to the tubule. This orientation is randomized in mice with cystic kidney disease caused by defects in the transcription factor hepatocyte nuclear factor 1β (Hnf1β) or by loss of Fat4, which disrupts planar cell polarity, and is less precise in rats with defects in the ciliary/centrosomal protein fibrocystin (Fischer et al., 2006; Saburi et al., 2008) or mice with mutations in the ciliary assembly protein Kif3a (Patel et al., 2008). To test if a lack of IFT20 caused a randomization of mitotic spindle orientation, we examined collecting duct mitosis in sections of p5 kidneys. p5 is just before the time of rapid cystic expansion (Fig. 1 B) and should be the point at which spindle orientation defects would be most evident. As described, there is some tubule dilation in p5 experimental animals. We were concerned that once tubule dilation had initiated, mitotic spindle orientation could be altered as a secondary effect, so we analyzed only those tubules that were not visibly dilated. Thus, at p5, tubule diameter was similar in control and experimental mice (control = 16.4 ± 0.24 µm; experimental = 17.0 ± 0.38 µm), as was the percentage of collecting ducts cells undergoing mitosis (control = 2.54 ± 0.67%; experimental = 2.58 ± 0.52%; $n = 5$ animals, >1,000 cortical collecting duct cells counted per animal). However, in the absence of IFT20, the normal bias toward spindle orientation being parallel to the long axis of the tubule was lost (Fig. 3 A), resulting in significantly different mitotic spindle orientations between control and experimental collecting duct cells (Fig. 3 B; $P < 0.001$).

To probe further how the lack of a cilium might lead to misorientation of the mitotic spindle, we examined centrosomal position. Normal kidney epithelial cells are highly polarized, with centrosomes typically located at the center of the apical end of the cell. This is typically the apex of the cell so that the cilium projects from the tip of the cell into the tubule (Fig. 4 A). Without IFT20, the centrosome is often displaced from the center of the apical surface of the cell (Fig. 4, A and B). In p5 mutants, the centrosome remains at the apical end of the cell but can be found

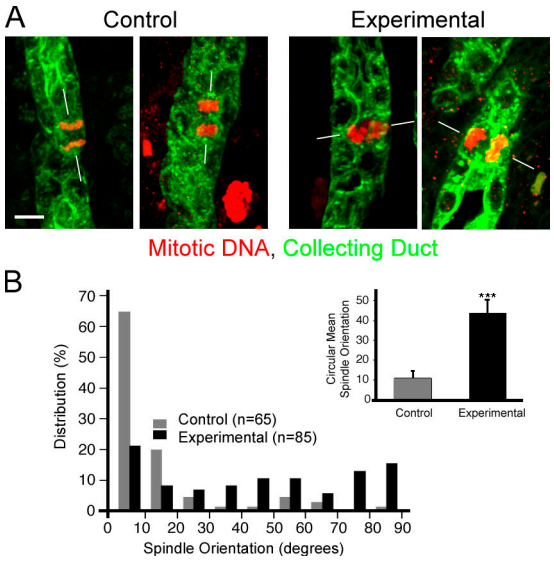

Figure 3. **Deletion of *Ift20* leads to mitotic spindle misorientation in p5 collecting duct cells.** (A) In normal kidney tubules, mitotic spindles (phospho-histone H3, red) typically orient their axes (white lines) parallel to the long axis of the collecting duct (DBA, green; left panels in A, gray bars in B). The absence of IFT20 disrupts this arrangement, producing a more random orientation of mitotic spindles (right panels in A, black bars in B). Images are maximum projections of 16 confocal z images taken 0.5 µm apart. Bar, 5 µm. (B) Mitotic spindle orientation quantitation. Mitotic collecting duct cells were photographed, and the angle between the long axis of the tubule and the spindle was measured; angles were grouped into 10° bins. Bars in the inset show circular mean mitotic spindle orientation and the 95% confidence interval about the mean. ***, $P < 0.001$ (Kolmogorov-Smirnov test).

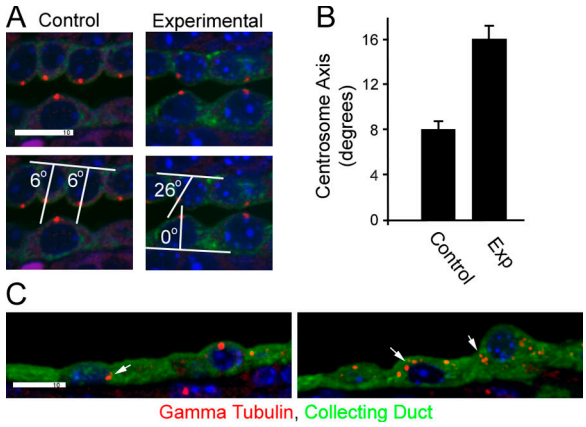

Figure 4. **Centrosome defects.** (A) In control p5 kidneys, centrosomes (γ-tubulin, red) are typically found at the center of the apical surface of collecting duct cells, whereas the position in experimental animals is more variable. The position was quantified by measuring the angle between a line along the basal surface of the cell and a line drawn between the centrosome and the center of the cell at the basal surface. The cell center was defined by the center of the nucleus. The bottom two panels illustrate this measurement. Images are maximum projections of four confocal z images taken 0.5 µm apart. (B) Quantification of the centrosome axis. $n = 100$. Error bars indicate SEM. (C) Two examples of the unusual localization of centrosomes (arrows) that can be found in highly cystic kidneys. Bars, 10 µm.

anywhere from the lateral junction to the center of the cell. In the highly cystic kidneys of older animals, centrosomal position varies along the apical-basal axis, often localizing near the basal surface (Fig. 4 C). The process of oriented cell division in the kidney may be analogous to what occurs in adult stem cells, which divide via oriented mitosis to maintain the stem cell niche and produce cells for differentiation. Work in *Drosophila melanogaster* stem cells indicates that centrosome dynamics underlie this process: the mother centrosome remains anchored at a fixed position in the cell and the daughter centrosome moves to a stereotypical position at the other side of the cell before the mitotic spindle is established. Mutations that disrupt the centrosomes disrupt the orientation of the mitotic spindle and lead to less-ordered cell division planes (Rebollo et al., 2007; Rusan and Peifer, 2007). If the process in kidney cells is similar to that in stem cells, the cilium may provide an external cue to position the mother centrosome, coordinating the cell division plane of an individual cell with neighboring tubular cells. In addition to mislocalized centrosomes, some cells lacking IFT20 showed centrosome overduplication or segregation defects, with large numbers of γ-tubulin–positive structures found throughout the cell (Fig. 4 C). This centrosomal amplification was not frequent, and cells with this phenotype were clustered together, which suggests that an additional mutation had occurred in a precursor cell that then gave rise to the cluster.

Mitotic spindle orientation is thought to be controlled by the noncanonical branch of the Wnt pathway, whereas the canonical branch controls gene expression through the interaction of β-catenin with T cell factor (Tcf) transcription factors (Merkel et al., 2007). Because we observed defects in mitotic spindle orientation, we sought to determine if β-catenin signaling was altered in *Ift20* mutant kidneys. At p10, β-catenin staining was similar in the collecting ducts and cysts of control and experimental animals (Fig. 5 A, top). However, cysts in adult experimental mice (p33) stained more strongly for β-catenin than did control collecting ducts (Fig. 5 A, bottom). To discern cellular distribution of β-catenin, Western blots of cytosolic and nuclear kidney fractions were probed with antibodies to β-catenin and to dephosphorylated β-catenin, which is competent to enter the nucleus and interact with the Tcf transcription regulatory complex. Total β-catenin levels in the cytoplasmic fraction were slightly elevated in experimental kidneys. Transcriptionally active β-catenin was highly elevated in the nuclear fractions of the experimental kidneys and was also faintly detected in mutant but not control kidney cytoplasm (Fig. 5 B).

To determine if elevated dephosphorylated β-catenin heralded changes in Wnt pathway gene expression, we used Wnt signaling quantitative real-time PCR (qPCR) arrays to query expression levels of 84 Wnt-related genes in four individual mutant and control kidneys. Expression of a subset of these genes was altered in mutants (Table S1, available at http://www.jcb.org/cgi/content/full/jcb.200808137/DC1). Most dramatic in mutant kidneys was a >200-fold increase in *Wnt7a*, a gene not previously linked to kidney development or disease. *Wnt7a* null mice are viable but sterile because of defects in Mullerian duct development. They also display skeletal defects such as missing digits and extra ribs but have not been reported to have kidney defects (Parr and McMahon, 1995). Other Wnt ligands (*Wnt7b*, *Wnt10a*, *Wnt 9a*, *Wnt6*, *Wnt 4*, and *Wnt2*) were also up-regulated

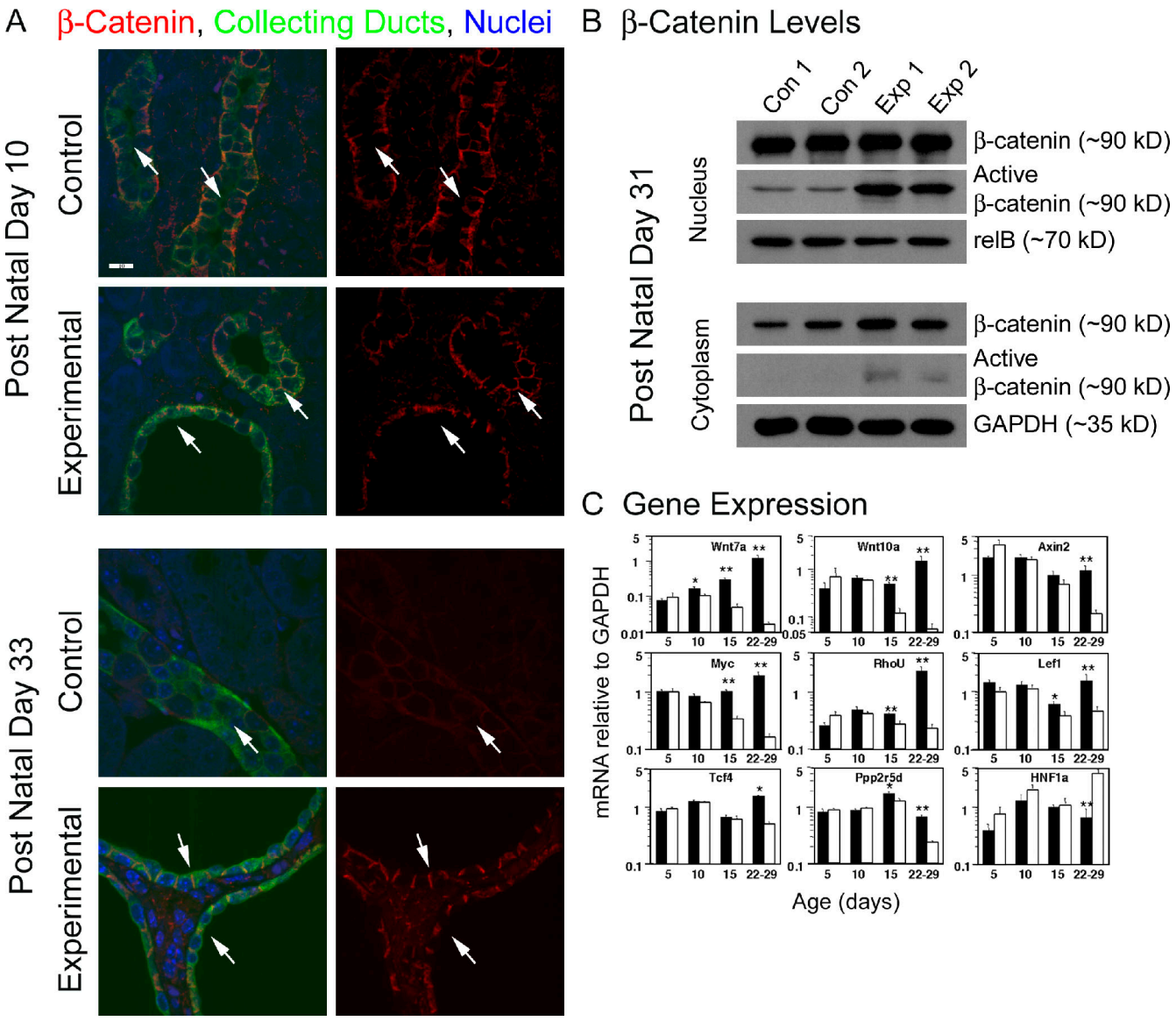

Figure 5. **Deletion of Ift20 alters canonical Wnt signaling.** (A) β-catenin staining of control (top rows) and experimental (bottom rows) kidneys at p10 and p33. Arrows indicate collecting ducts in controls and dilated or cystic ducts in experimental mice. Images are maximum projections of five confocal z images taken 0.5 µm apart (2 µm total). Control and experimental images at each of the time points were taken under identical conditions and manipulated uniformly, but the conditions were not the same at p10 and p33. Bar, 10 µm. (B) Western blot analysis of β-catenin. Control (Con) and experimental (Exp) kidneys were separated into cytosol and nuclear fractions and analyzed by Western blots with antibodies to β-catenin and dephosphorylated (active) β-catenin. RelB and GAPDH were used as loading controls. "1" and "2" represent different animals. (C) qPCR analysis of nine genes in experimental (closed bars) and control (open bars) kidneys at selected postnatal times. Gene expression data are normalized to GAPDH expression. Bars indicate mean ± SEM of 5–11 mice in each treatment and age group, plotted on logarithmic scales. *, $P < 0.05$; **, $P < 0.01$ (unpaired *t* tests).

in mutant kidneys, along with Wnt-binding proteins (*Frz6* and *Frzb*). Downstream Wnt signaling targets *Myc*, *Jun*, *Tcf3*, *Tcf7*, and *Wisp1* increased, as did other genes such *Rhou* and *PPP2r5d*. *Rhou* is a member of the Rho subfamily of small GTPases. Its overexpression causes disassembly of focal adhesions (Chuang et al., 2007) and causes quiescent fibroblasts to enter the cell cycle (Tao et al., 2001), phenotypes that may be important in the formation of kidney cysts. Ppp2r5d is a regulatory subunit of protein phosphatase 2, which plays a role in regulating entry into mitosis (Margolis et al., 2006).

Recent data on kidney development indicates that cilia and polycystins play vital roles in the embryonic and postnatal development of the kidney but may not be critical in the adult. The transition point for this ciliary dependence appears to occur in the p10–14 range (Piontek et al., 2007; Patel et al., 2008), which led us to ask if Wnt-related gene expression changes over this time period. We followed expression of a subset of the genes on the array, plus additional genes known to be associated with Wnt signaling, through postnatal development (p5, p10, and p15) and into early adulthood (p22–29). Consistent with a p10–p14 ciliary dependence transition, expression levels of most of the interrogated genes at p5 or p10 did not differ between mutant and control kidneys, with the exception of *Wnt7a*, whose expression was modestly but significantly increased at p10. In contrast,

significant increases in expression of many genes, including *Wnt7a*, *Wnt10a*, *Myc*, *RhoU*, *Lef1*, and *Ppp2r5d* mRNAs, were seen in p15 mutant kidneys (Fig. 5 C). The relative differences in expression of these genes increased in young adult mice by combined up-regulation in mutant kidneys and decreased expression in controls. *Axin2* and *Tcf4*, two genes associated with β-catenin activation, were up-regulated only in highly cystic young adult mice. In contrast, expression of HNF1α significantly decreased in young adult mutant kidney; mutations in HNF1α have been associated with some human renal malformations, although HNF1β abnormalities are more commonly linked to PKD (Malecki et al., 2005). How these changes in Wnt-related gene expression influence cyst formation warrants further study.

One functional consequence of up-regulated Wnt–β-catenin signaling is increased proliferation (Morin, 1999). As discussed, we did not observe differences in proliferation at p5, but adult cystic epithelium showed increased proliferation as measured by phospho-histone staining (control = 0.54 ± 0.12%; experimental = 3.87 ± 0.43%; $n = 5$ animals, >1,000 DBA-positive cortical collecting duct cells counted from each animal, $P < 0.0001$; unpaired t test).

Work in several model systems supports the hypothesis that cilia play a key role in cystic disease, but the nature of that role remains an open question. Cilia often serve as chemoreceptors (e.g., in olfaction). Although this is theoretically a possibility in the kidney, there is as yet no evidence to support this idea. Cilia can also serve as mechanosensors (Praetorius and Spring, 2001). The observation that responses to flow are aberrant in cells lacking the polycystins has been used to argue that the cilium dynamically monitors flow through the tubule and uses this information to control tubule diameter and prevent cyst formation (Nauli et al., 2003). However, the observation that cilia are not required in adult animals (Davenport et al., 2007) and that cells lacking the transient receptor potential (Trp) channel TrpV4 do not respond to flow but that mice and fish lacking this gene do not develop cystic disease (Kottgen et al., 2008) calls into question the importance of dynamic flow detection to cystogenesis. Another possible function for the cilium is to regulate Wnt signaling. Wnt signaling is involved in early kidney development (Merkel et al., 2007), and the finding that expression of an activated, mutant form of β-catenin in kidney epithelium leads to cystic disease (Saadi-Kheddouci et al., 2001) suggested that defects in Wnt–β-catenin signaling underlie the transformation of a normal tubule into a cyst. More recent data show dysregulation of the Wnt–β-catenin signaling pathway in other models of cystic kidney disease, and it has been proposed that one of the functions of cilia is to regulate the switch between canonical and noncanonical Wnt signaling upon fluid flow through the nephron (Simons et al., 2005; Corbit et al., 2008; Marose et al., 2008). This idea is based partly on the observation that canonical Wnt signaling is high in tip cells of the invading ureteric bud that are not expected to be exposed to fluid flow, whereas it is low in trunk cells that are more likely to be exposed to flow (Simons and Walz, 2006). Our data supports a role for the cilium in regulating both the canonical and noncanonical branches of the Wnt pathway, although this regulation may be more complex than a switch between the two branches. It is more likely that the cilium provides spatial information to control noncanonical Wnt signaling at all postnatal time periods and also provides information to down-regulate canonical Wnt signaling at p15 and later.

It is possible that both canonical and noncanonical branches of Wnt signaling need to be upset for cyst formation to occur. That is, altered mitotic spindle orientation without an increase in proliferation could cause cells to divide in random planes, resulting in shorter tubules that are somewhat dilated but not greatly cystic. Conversely, increased proliferation with correct orientation of cell division could lead to longer tubules of the correct diameter. However, when altered mitotic orientation is combined with increased proliferation, dramatic cyst formation occurs.

Materials and methods

Histology

Mouse tissues for histological analysis were fixed by perfusion (>10 d of age) or immersion with either 4% paraformaldehyde (Electron Microscopy Sciences) or 2% glutaraldehyde (Electron Microscopy Sciences), plus 4% paraformaldehyde in phosphate-buffered saline and then embedded in paraffin. Sections were deparaffinized, and antigens were retrieved by boiling for 15 min in sodium citrate, pH 6.0, and stained with primary antibodies diluted in TBST (10 mM Tris, pH 7.5, 167 mM NaCl, and 0.05% Tween 20) plus 0.1% cold water fish skin gelatin (Sigma-Aldrich). Tissues for scanning electron microscopy were perfused with 4% paraformaldehyde plus 2% glutaraldehyde in PBS and prepared as described previously (Pazour et al., 2000).

Alexa Fluor–labeled secondary antibodies (Invitrogen) were used to detect the primary antibodies. Primary antibodies used included acetylated tubulin (611-β-1, 1:10,000; Sigma-Aldrich), γ-tubulin (GTU88, 1:1,000; Sigma-Aldrich), smooth muscle actin (clone 1A4, 1:50,000; Sigma-Aldrich), phospho-histone $H3^{Ser10}$ (1:250; Millipore), aquaporin 2 (1:500; BD Biosciences), β-catenin (1:1,000; Cell Signaling Technology), active β-catenin (clone 8E7, 1:300; Upstate Biotechnology), glyceraldehyde 3-phosphate dehydrogenase (GAPDH; clone 14C10, 1:1,000; Cell Signaling Technology), RelB (N-17, 1:250; Santa Cruz Biotechnology, Inc.). FITC-conjugated DBA (1:20; Sigma-Aldrich) was added with the secondary antibodies. Trichrome blue staining was performed by using the Accustain Trichrome stain kit (Masson; Sigma-Aldrich).

Wide-field images were acquired by an Orca ER camera (Hamamatsu) on a microscope (Axiovert 200M; Carl Zeiss, Inc.) equipped with a 100× Plan-Apochromat 1.4 NA objective (Carl Zeiss, Inc.). Images were captured by Openlab software (Improvision) and adjusted for contrast in Photoshop (Adobe). To compare images, photos were taken with identical conditions and manipulated equally. Confocal images were acquired with an inverted microscope (TE-2000E2; Nikon) equipped with a Solamere Technology–modified spinning disk confocal scan head (CSU10; Yokogawa). z stacks were acquired at 0.5-µm intervals and converted to single planes by maximum projection with MetaMorph software (MDS Analytical Technologies). Bright-field images were acquired using a microscope (Axioskop 2 Plus) equipped with a color digital camera (Axiocam HRC) and acquisition software (Axiovision 4.0; all from Carl Zeiss, Inc.).

Gene targeting and mouse breeding

A gene targeting vector to modify the mouse IFT20 locus was developed using bacterial recombination (May et al., 2005). In brief, 7.6 kb of DNA from mouse BAC RP23-3999H5 (Children's Hospital of Oakland Research Institute) was captured into pL253. Additional recombination steps placed LoxP sites in introns 1 and 3 and a neomycin selectable marker flanked by flipase recognition target recombination sites in intron 1. This construct was electroporated into mouse embryonic stem cell line AB2.2. Correctly targeted lines were identified by PCR and used to generate chimeric mice that were bred to produce a line carrying the $ift20^{neo}$ allele. FLPe (Farley et al., 2000), Prm-Cre (O'Gorman et al., 1997), and HoxB7-Cre (Yu et al., 2002) mice were obtained from the Jackson Laboratory.

Mice carrying the $ift20^{neo}$ allele were crossed to FLPe mice to delete the neomycin selectable marker and create the $ift20^{flox}$ allele. These were subsequently crossed to Prm-Cre mice to delete exons 2 and 3 and create the $ift20^{null}$ allele. Homozygous $ift20^{flox}$ and homozygous $ift20^{neo}$ mice are viable and fertile, and these lines are maintained as homozygotes. Homozygous $ift20^{null}$ mice do not survive to birth, and this line is maintained by heterozygote crosses.

Table I. **RT-qPCR primers**

Primer	Accession no.	Sequence	Tm	Amplicon
			°C	*bp*
MmAxin2Exon3For	NM_027732	GACGCACTGACCGACGATTCCA	61.5	120
MmAxin2Exon4Rev		ATTGGCCTTCACACTGCGATGC	60.7	
MmGAPDHExon3For	NM_008084	GCAATGCATCCTGCACCACCA	61.1	138
MmGAPDHExon4Rev		TTCCAGAGGGGCCATCCACA	61.1	
MmHNF1aExon5For	NM_009327	CGCGTGGCGAAGATGGTCAAGT	62.3	124
MmHNF1aExon6Rev		TCATGGGTGTGCCCTTGTTGAGG	61.8	
MmLef1Exon3For	NM_010703	TTCTCCACCCATCCCGAGGACA	62.1	122
MmLef1Exon4Rev		ACGGGTGGGATCCCGGAGAAAA	62.8	
MmMycExon2For	NM_010849	CACCACCAGCAGCGACTCTGAA	61.7	125
MmMycExon3Rev		TGTGGCCTCGGGATGGAGATGA	62.4	
MmPpp2r5dExon11For	NM_009358	CGCATCCTCCCCATCATGTTTCC	60.2	135
MmPpp2r5dExon12Rev		TGTGCAGTCGTCAAACAGCTTCTGG	61.5	
MmRhoUExon2For	NM_133955	TGTAGATGGGCGGCCTGTGAGA	62.5	119
MmRhoUExon3Rev		CCACGCTGAAGCACAGCAGGAA	62.4	
MmTcf4Exon7For	NM_013685	GGGCAATCCAGGAACCCTTTCG	60.6	150
MmTcf4Exon8Rev		GAAGACGGCAAACCCGGAGGAA	61.8	
MmWnt7aExon3For	NM_009527	GATGCCCGGGAGATCAAGCAGA	61.3	122
MmWnt7aExon4Rev		GAGCCTGACACACCATGGCACT	61.9	
MmWnt10aExon1For	NM_009518	TTCTGGGCGCTCCTGTTCTTCC	61.7	123
MmWnt10aExon2Rev		CAGGCACACTGTGTTGGCGTTG	61.6	

These sequence data are available from GenBank/EMBL/DDBJ under the accession numbers listed. Tm, melting temperature.

Genotyping was done by PCR using the following primers as described in Fig. S1: (A) 5′-ACTCAGTATGCAGCCCAGGT-3′, (B) 5′-GCTAGATGCTGGGCGTAAAG-3′, (C) 5′-GGGGAACTTCCTGACTAGGG-3′, and (D) 5′-GGAGCCAGGTTCAGTTATGC-3′.

Mice with kidney collecting duct deletion of IFT20 were generated by crossing HoxB7-Cre, *ift20*$^{null/+}$ males to *ift20*$^{flox/flox}$ females. Offspring with the genotype HoxB7-Cre, *ift20*$^{null/flox}$ were used as experimental animals, whereas HoxB7-Cre, *ift20*$^{+/flox}$ were used as controls. Mouse work was approved by the University of Massachusetts Medical School animal use committee.

Serum chemistry

Blood urea nitrogen was analyzed by a Cobra Integra 400 Plus (Roche) at the Comparative Pathology Laboratory, Baylor College of Medicine.

Cell fractionation and protein analysis

Kidney cytoplasmic and nuclear extracts were prepared using the CelLytic NuCLEAR Extraction kit (Sigma-Aldrich) protocol. For Western blot analysis, proteins were separated by SDS-PAGE and electrotransferred to Immobilon P (Millipore). After transfer, blots were blocked with TBST containing 5% dry milk and then incubated with primary antibodies in the same solution.

Gene expression

Individual kidneys were stored at −80°C in RNAlater (QIAGEN) until total RNA was isolated (QiaShredder columns, RNeasy kits with on-column DNA digestion; QIAGEN). RNA concentration was determined spectrophotometrically. Wnt-related gene expression was examined with the mouse Wnt signaling pathway RT^2 profiler PCR arrays (PAMM-043C; SABiosciences) using cDNA (Reaction Ready First-Strand cDNA Synthesis kit; SABiosciences) derived from four experimental and four control kidneys. Thermal cycling was performed in an ABI Prism 7500 instrument (Applied Biosystems). Fold changes in gene expression were calculated (http://www.sabiosciences.com/pcr/arrayanalysis.php) after normalizing data to the array's five housekeeping gene pool.

To analyze gene expression at selected postnatal times, qPCR was used with gene-specific primers. Primers were designed with Primer3 and IDT tools (http://fokker.wi.mit.edu/primer3/input.htm and http://www.idtdna.com/Scitools/Applications/Primerquest/). PCR was performed with an ABI Prism 7500 (Applied Biosystems) using 15-µl reactions containing 2.5 ng of first strand cDNA (SuperScript II First-Strand Synthesis System; Invitrogen), 0.5 µM forward and reverse primers, and PowerSYBR green PCR master mix (Applied Biosystems). qPCR reactions were performed in duplicate or triplicate at 50°C for 2 min, 95°C for 10 min, 40 cycles at 95°C for 15 s, and 60°C for 60 s, then dissociated to verify a single amplicon. For each gene, standard curves were generated from a 10-fold serially diluted (250 ng to 2.5 pg) pool of p22–29 ift20 null/flox kidney cDNA. Threshold cycle (CT) was calculated for each point, standard curves related CT to log cDNA dilution, and RNA abundance was estimated by relating sample CT to the standard curve. qPCR data were normalized to GAPDH expression. RT-qPCR information is shown in Table I.

Data analysis

Tubular diameter, mitotic index, centrosomal angles, and gene expression are presented as means ± SEM, and were compared between experimental and control mice with unpaired *t* tests. Differences between groups were considered statistically significant if $P < 0.05$. Circular mean mitotic spindle orientation and 95% confidence intervals (CI) were calculated using the von Mises distribution (Fisher, 1993), and the Kolmogorov-Smirnov two-sample test (Daniel, 1990) was used to discern significant differences.

Online supplemental material

Fig. S1 describes the construction of the *Ift20* mutant mouse and genotyping details. Fig. S2 illustrates fibrosis and the presence of smooth muscle actin-positive cells in the mutant kidneys. Table S1 provides the entire set of Wnt-related genes that were analyzed by PCR array. Online supplemental material is available at http://www.jcb.org/cgi/content/full/jcb.200808137/DC1.

We thank M. Keeler and Dr. S. Jones (University of Massachusetts Medical School [UMMS] Transgenic Core Facility) for assistance with generation of *Ift20* alleles; Dr. P. Furcinitti (UMMS Digital Imaging Core Facility) for assistance with confocal imaging; Dr. P. Odgren for use of his bright field microscope; Drs. K. McDermott, R. Davis, and C. Weston for assistance with histological analysis; and Drs. C. Mello and J. Claycomb for assistance with real-time PCR. We also thank F. Xu for technical assistance and S. Baker for statistical analysis of mitotic spindle orientation.

This work was supported by the National Institutes of Health (grant GM060992), the Iacocca Foundation, the Order of the Eagles (to G.J. Pazour), and the Polycystic Kidney Disease Foundation (to J.A. Jonassen). Core resources supported by the Diabetes Endocrinology Research Center (grant DK32520) were also used.

Submitted: 25 August 2008
Accepted: 1 October 2008

References

Chuang, Y.Y., A. Valster, S.J. Coniglio, J.M. Backer, and M. Symons. 2007. The atypical Rho family GTPase Wrch-1 regulates focal adhesion formation and cell migration. *J. Cell Sci.* 120:1927–1934.

Corbit, K.C., A.E. Shyer, W.E. Dowdle, J. Gaulden, V. Singla, and J.F. Reiter. 2008. Kif3a constrains beta-catenin-dependent Wnt signalling through dual ciliary and non-ciliary mechanisms. *Nat. Cell Biol.* 10:70–76.

Daniel, W.W. 1990. Applied Nonparametric Statistics. Second Edition. Pacific Grove, CA: Duxbury Thomson Learning. 635 pp.

Davenport, J.R., A.J. Watts, V.C. Roper, M.J. Croyle, T. van Groen, J.M. Wyss, T.R. Nagy, R.A. Kesterson, and B.K. Yoder. 2007. Disruption of intraflagellar transport in adult mice leads to obesity and slow-onset cystic kidney disease. *Curr. Biol.* 17:1586–1594.

Farley, F.W., P. Soriano, L.S. Steffen, and S.M. Dymecki. 2000. Widespread recombinase expression using FLPeR (flipper) mice. *Genesis.* 28:106–110.

Fischer, E., E. Legue, A. Doyen, F. Nato, J.F. Nicolas, V. Torres, M. Yaniv, and M. Pontoglio. 2006. Defective planar cell polarity in polycystic kidney disease. *Nat. Genet.* 38:21–23.

Fisher, N.I. 1993. Statistical Analysis of Circular Data. New York: Cambridge University Press. 295 pp.

Igarashi, P., and S. Somlo. 2002. Genetics and pathogenesis of polycystic kidney disease. *J. Am. Soc. Nephrol.* 13:2384–2398.

Kottgen, M., B. Buchholz, M.A. Garcia-Gonzalez, F. Kotsis, X. Fu, M. Doerken, C. Boehlke, D. Steffl, R. Tauber, T. Wegierski, et al. 2008. TRPP2 and TRPV4 form a polymodal sensory channel complex. *J. Cell Biol.* 182:437–447.

Malecki, M.T., J. Skupien, S. Gorczynska-Kosiorz, T. Klupa, J. Nazim, D.K. Moczulski, and J. Sieradzki. 2005. Renal malformations may be linked to mutations in the hepatocyte nuclear factor-1alpha (MODY3) gene. *Diabetes Care.* 28:2774–2776.

Margolis, S.S., J.A. Perry, C.M. Forester, L.K. Nutt, Y. Guo, M.J. Jardim, M.J. Thomenius, C.D. Freel, R. Darbandi, J.H. Ahn, et al. 2006. Role for the PP2A/B56delta phosphatase in regulating 14-3-3 release from Cdc25 to control mitosis. *Cell.* 127:759–773.

Marose, T.D., C.E. Merkel, A.P. McMahon, and T.J. Carroll. 2008. Beta-catenin is necessary to keep cells of ureteric bud/Wolffian duct epithelium in a precursor state. *Dev. Biol.* 314:112–126.

May, S.R., A.M. Ashique, M. Karlen, B. Wang, Y. Shen, K. Zarbalis, J. Reiter, J. Ericson, and A.S. Peterson. 2005. Loss of the retrograde motor for IFT disrupts localization of Smo to cilia and prevents the expression of both activator and repressor functions of Gli. *Dev. Biol.* 287:378–389.

Merkel, C.E., C.M. Karner, and T.J. Carroll. 2007. Molecular regulation of kidney development: is the answer blowing in the Wnt? *Pediatr. Nephrol.* 22:1825–1838.

Morin, P.J. 1999. beta-catenin signaling and cancer. *Bioessays.* 21:1021–1030.

Nauli, S.M., F.J. Alenghat, Y. Luo, E. Williams, P. Vassilev, X. Li, A.E. Elia, W. Lu, E.M. Brown, S.J. Quinn, et al. 2003. Polycystins 1 and 2 mediate mechanosensation in the primary cilium of kidney cells. *Nat. Genet.* 33:129–137.

O'Gorman, S., N.A. Dagenais, M. Qian, and Y. Marchuk. 1997. Protamine-Cre recombinase transgenes efficiently recombine target sequences in the male germ line of mice, but not in embryonic stem cells. *Proc. Natl. Acad. Sci. USA.* 94:14602–14607.

Parr, B.A., and A.P. McMahon. 1995. Dorsalizing signal Wnt-7a required for normal polarity of D-V and A-P axes of mouse limb. *Nature.* 374:350–353.

Patel, V., L. Li, P. Cobo-Stark, X. Shao, S. Somlo, F. Lin, and P. Igarashi. 2008. Acute kidney injury and aberrant planar cell polarity induce cyst formation in mice lacking renal cilia. *Hum. Mol. Genet.* 17:1578–1590.

Pazour, G.J. 2004. Intraflagellar transport and cilia-dependent renal disease: the ciliary hypothesis of polycystic kidney disease. *J. Am. Soc. Nephrol.* 15:2528–2536.

Pazour, G.J., B.L. Dickert, Y. Vucica, E.S. Seeley, J.L. Rosenbaum, G.B. Witman, and D.G. Cole. 2000. *Chlamydomonas IFT*88 and its mouse homologue, polycystic kidney disease gene *Tg737*, are required for assembly of cilia and flagella. *J. Cell Biol.* 151:709–718.

Piontek, K., L.F. Menezes, M.A. Garcia-Gonzalez, D.L. Huso, and G.G. Germino. 2007. A critical developmental switch defines the kinetics of kidney cyst formation after loss of Pkd1. *Nat. Med.* 13:1490–1495.

Praetorius, H.A., and K.R. Spring. 2001. Bending the MDCK cell primary cilium increases intracellular calcium. *J. Membr. Biol.* 184:71–79.

Rebollo, E., P. Sampaio, J. Januschke, S. Llamazares, H. Varmark, and C. Gonzalez. 2007. Functionally unequal centrosomes drive spindle orientation in asymmetrically dividing *Drosophila* neural stem cells. *Dev. Cell.* 12:467–474.

Rosenbaum, J.L., and G.B. Witman. 2002. Intraflagellar transport. *Nat. Rev. Mol. Cell Biol.* 3:813–825.

Rusan, N.M., and M. Peifer. 2007. A role for a novel centrosome cycle in asymmetric cell division. *J. Cell Biol.* 177:13–20.

Saadi-Kheddouci, S., D. Berrebi, B. Romagnolo, F. Cluzeaud, M. Peuchmaur, A. Kahn, A. Vandewalle, and C. Perret. 2001. Early development of polycystic kidney disease in transgenic mice expressing an activated mutant of the beta-catenin gene. *Oncogene.* 20:5972–5981.

Saburi, S., I. Hester, E. Fischer, M. Pontoglio, V. Eremina, M. Gessler, S.E. Quaggin, R. Harrison, R. Mount, and H. McNeill. 2008. Loss of Fat4 disrupts PCP signaling and oriented cell division and leads to cystic kidney disease. *Nat. Genet.* 40:1010–1015.

Satir, P., and S.T. Christensen. 2007. Overview of structure and function of mammalian cilia. *Annu. Rev. Physiol.* 69:377–400.

Scholey, J.M. 2003. Intraflagellar transport. *Annu. Rev. Cell Dev. Biol.* 19:423–443.

Simons, M., and G. Walz. 2006. Polycystic kidney disease: cell division without a c(l)ue? *Kidney Int.* 70:854–864.

Simons, M., J. Gloy, A. Ganner, A. Bullerkotte, M. Bashkurov, C. Kronig, B. Schermer, T. Benzing, O.A. Cabello, A. Jenny, et al. 2005. Inversin, the gene product mutated in nephronophthisis type II, functions as a molecular switch between Wnt signaling pathways. *Nat. Genet.* 37:537–543.

Tao, W., D. Pennica, L. Xu, R.F. Kalejta, and A.J. Levine. 2001. Wrch-1, a novel member of the Rho gene family that is regulated by Wnt-1. *Genes Dev.* 15:1796–1807.

Yu, J., T.J. Carroll, and A.P. McMahon. 2002. Sonic hedgehog regulates proliferation and differentiation of mesenchymal cells in the mouse metanephric kidney. *Development.* 129:5301–5312.